Field-Scale Effective Matrix Diffusion Coefficient for Fractured Rock: Results From Literature Survey

Quanlin Zhou [1], Hui-Hai Liu [1], Fred J. Molz [2], Yingqi Zhang [1], and Gudmundur S. Bodvarsson [1]

[1]Earth Sciences Division, Lawrence Berkeley National Laboratory, University of California, Berkeley, California 94720.

[2]Department of Environmental Engineering and Science, Clemson University, Clemson, South Carolina 29634

March 2005

Abstract

Matrix diffusion is an important mechanism for solute transport in fractured rock. We recently conducted a literature survey on the effective matrix diffusion coefficient, D_m^e, a key parameter for describing matrix diffusion processes at the field scale. Forty field tracer tests at 15 fractured geologic sites were surveyed and selected for study, based on data availability and quality. Field-scale D_m^e values were calculated, either directly using data reported in the literature or by reanalyzing the corresponding field tracer tests. Surveyed data indicate that the effective-matrix-diffusion-coefficient factor F_D (defined as the ratio of D_m^e to the lab-scale matrix diffusion coefficient [D_m] of the same tracer) is generally larger than one, indicating that the effective matrix diffusion coefficient in the field is comparatively larger than the matrix diffusion coefficient at the rock-core scale. This larger value could be attributed to the many mass-transfer processes at different scales in naturally heterogeneous, fractured rock systems. Furthermore, we observed a moderate trend toward systematic increase in the F_D value with observation scale, indicating that the effective matrix diffusion coefficient is likely to be statistically scale dependent. The F_D value ranges from 1 to 10,000 for observation scales from 5 to 2,000 m. At a given scale, the F_D value varies by two orders of magnitude, reflecting the influence of differing degrees of fractured rock heterogeneity at different sites. In addition, the surveyed data indicate that field-scale longitudinal dispersivity generally increases with observation scale, which is consistent with previous studies. The scale-dependent field-scale matrix diffusion coefficient (and dispersivity) may have significant implications for assessing long-term, large-scale radionuclide and contaminant transport events in fractured rock, both for nuclear waste disposal and contaminant remediation.

1. Introduction

The phenomenon of matrix diffusion in fractured rock has been the subject of considerable research interest over the past three decades since *Foster* [1975] used it to interpret a groundwater tritium anomaly in field observations [e.g., *Grisak and Pickens*, 1980; *Neretnieks*, 1980]. Direct laboratory and field evidence of matrix diffusion, defined originally as molecular diffusive mass transfer of a solute between flowing fluid within fractures and stagnant fluid in the rock matrix, has been obtained in terms of an observed solute penetration distance into a rock matrix [e.g., *Birgersson and Neretnieks*, 1990; *Jardine et al.*, 1999; *Polak et al*., 2003]. Indirect evidence has been obtained from multi-tracer tests through the significant breakthrough-curve separation of simultaneously injected tracers of different matrix-diffusion-coefficient values [e.g., *Garnier et al*., 1985; *Maloszewski et al*., 1999; *Karasaki et al*., 2000; *Reimus et al.*, 2003a, b]. In a rock matrix not containing tiny cracks, molecular diffusion would be the dominant transport process, with negligible fluid velocity and thus dispersion; within fractures, advection and dispersion are the two dominant transport processes [e.g., *Tang et al*., 1981; *Sudicky and Frind*, 1982; *Maloszewski and Zuber*, 1990, 1993; *Moench*, 1995]. It is well documented in the literature that matrix diffusion is an important process for retarding solute transport in fractured rock, by allowing for solute storage within the often large void space of the matrix [e.g., *Neretnieks*, 1980; *Zhou et al*., 2003].

The matrix diffusion coefficient is a key parameter, both for describing the diffusion process in the rock matrix and diffusive mass transfer between fractures and the matrix. Laboratory experiments on rock-matrix cores and field tracer tests at a larger scale have been often employed to estimate this coefficient [e.g., *Skagius and Neretnieks*, 1986; *Ohlsson and Neretnieks*, 1995; *Ohlsson et al*., 2001; *Reimus et al*., 2003b]. It has been found that the lab-scale matrix diffusion coefficient may be orders of magnitude smaller than a field-scale value for the same geologic site, indicating that matrix diffusion in the field is enhanced in some way [e.g., *Hodgkinson and Lever*, 1983; *Maloszewski and Zuber*, 1993; *Shapiro*, 2001; *Neretnieks*, 2002; *Liu et al*., 2003, 2004a; *Andersson et al*., 2004]. The enhancement may also be related to the significant inconsistency between rock properties (e.g., fracture aperture and matrix porosity) estimated from field tracer tests and those measured directly or estimated from hydraulic tests [e.g., *Novakowski et al.*, 1985]. The observed enhancement has been attributed to different mechanisms, including the existence of a degradation zone near the fracture-matrix interface [*Hodgkinson and Lever*, 1983; *Zhou et al*., 2005], infilling materials and stagnant water within fractures [*Johns and Roberts*, 1991; *Maloszewski and Zuber*, 1993; *Neretnieks*, 2002], the effects of small-scale fractures [*Wu et al*., 2004], advective mass transfer between high- and low-permeability zones [*Shapiro*, 2001], and the potential fractal structure of transport paths in a fracture network [*Liu et al*., 2004b]. By compiling field-

scale effective matrix-diffusion-coefficient values at several geologic sites, *Liu et al.* [2004b] found that for fractured rock, the field-scale matrix diffusion coefficient might be scale dependent. However, a comprehensive literature survey of the field-scale matrix diffusion coefficient in fractured rock is needed to further evaluate the potential scale-dependent behavior.

Many field tracer tests have been conducted in fractured rock since 1970 [e.g., *Webster et al*., 1970; *Ivanovich and Smith*, 1978; *Garnier et al*., 1985; *Raven et al*., 1988; *Cacas et al*., 1990b; *Gustafsson and Andersson*, 1991; *Hadermann and Heer*, 1996; *Becker and Shapiro*, 2000; *Reimus et al*., 2003a, b]. A few long-term, large-scale contaminant transport events have also been observed in fractured rock systems [e.g., *Bibby*, 1981; *Rudolph et al*., 1991; *Shapiro*, 2001]. These field tests and observations provide valuable data for investigating the field-scale matrix diffusion coefficient at different scales.

The objective of this study was to conduct a comprehensive literature survey of the field-scale matrix diffusion coefficient and to examine its potential scale-dependent behavior. For studies with reported effective matrix diffusion coefficients (D_m^e) from field tracer-test analysis, the reported D_m^e values were directly cited; for those without the reported D_m^e values, reanalysis of the tracer tests was conducted to obtain the D_m^e values. The reported and reanalyzed D_m^e values were presented as a function of observation scale to examine a potential relationship between the effective matrix diffusion coefficient and observation scale. With these goals in mind, we organize this paper as follows: (1) methods used to analyze field tracer tests (to obtain the effective matrix diffusion coefficient) are discussed in Section 2; (2) the effective matrix-diffusion-coefficient values determined from different field tests are presented in Section 3; (3) interpretations of the data for the effective matrix diffusion coefficient (and dispersivity) are provided in Section 4.

2. Determination of the Field-Scale Matrix Diffusion Coefficient

For the field tracer tests without reported D_m^e values, reanalysis of the tracer breakthrough curves was needed to calibrate transport parameters that included the effective matrix diffusion coefficient. This reanalysis was conducted using an analytic solution for linear flow and a semi-analytic solution for radial flow [*Maloszewski and Zuber*, 1985, 1990; *Reimus et al*., 2003b]. These analytic solutions and similar solutions [e.g., *Tang et al*., 1981; *Sudicky and Frind*, 1982; *Novakowski*, 1992] have been used for calibrating the D_m^e values reported in the literature.

2.1. Tracer Transport Model in Radial Flow

For reanalyzing tracer tests conducted in a two-well induced flow configuration, we used the semi-analytic solution for a parallel-fracture system [*Reimus et al*., 2003b]. The transport equations for both fractures and the matrix in a radial flow system can be written as follows:

$$\frac{\partial c_f}{\partial t} + \frac{v(r)}{R_f}\frac{\partial c_f}{\partial r} - \left(\frac{1}{R_f r}\right)\frac{\partial}{\partial r}\left(rD\frac{\partial c_f}{\partial r}\right) - \frac{\phi_m D_m}{bR_f}\frac{\partial c_m}{\partial x}|_{x=b} = 0\,, \tag{1}$$

$$\frac{\partial c_m}{\partial t} - \frac{D_m}{R_m}\frac{\partial^2 c_m}{\partial x^2} = 0, \quad b \le x \le B\,, \tag{2}$$

where subscripts f and m refer to fractures and the matrix, respectively, $c_f = c_f(r,t)$ and $c_m = c_m(r, x, t)$ are the solute concentrations, v is the groundwater velocity in fractures, R_f and R_m are the retardation factors, assuming a linear adsorption isotherm and instantaneous equilibrium, D is the hydrodynamic dispersion tensor, ϕ_m is the matrix porosity, D_m is the matrix diffusion coefficient, b is the half fracture aperture, r is the radial coordinate along fractures, x is the coordinate perpendicular to the fracture plane, t is time, and B is the half fracture spacing between neighboring parallel fractures.

The initial and boundary conditions for solute transport in fractures and the matrix can be written as follows:

$$c_f(r,0) = c_m(r,x,0) = 0\,, \tag{3.1}$$

$$c_f(0,t) = \begin{cases} \dfrac{M}{Qt_P}, & t \le t_p \\ 0, & t > t_p \end{cases} \tag{3.2}$$

$$c_f(\infty,t) = 0\,, \tag{3.3}$$

$$c_m(r,b,t) = c_f(r,t)\,, \tag{3.4}$$

$$\frac{\partial c_m(r,B,t)}{\partial x} = 0\,, \tag{3.5}$$

where M is the total mass of a tracer (or activity of a radioactive tracer) injected during $(0, t_p)$, t_p is the duration of mass injection, and Q is the pumping rate. Note that other

types of injection function can be derived using a very small t_p (for instantaneous injection) or a very large t_p (for constant-concentration injection).

By transforming and manipulating the transport equations, Equations (1) and (2), and the initial and boundary conditions, Equation (3), the analytic solution of the Laplace transform, $\overline{C}_f(s)$, of fracture concentration [*Becker and Charbeneau*, 2000; *Reimus et al.*, 2003b], can be written as:

$$\overline{C}_f(s) = \frac{M}{Qt_p}\left(\frac{1-\exp(-t_p s)}{s}\right)\exp\left(\frac{P_e}{2}\left(1-r_{wL}\right)\right)\frac{Ai\left(\sigma^{1/3}\left(P_e+\frac{1}{4\sigma}\right)\right)}{Ai\left(\sigma^{1/3}\left(r_{wL}P_e+\frac{1}{4\sigma}\right)\right)} \tag{4}$$

with

$$\sigma = \frac{2T_0}{P_e^2}\frac{s}{1-r_{wL}^2}\left[R_f + \frac{A}{\sqrt{s}}Tanh\left(\frac{R_m R_\phi}{A}\sqrt{s}\right)\right], \tag{5}$$

and the following set of transport parameters:

$$T_0 = r_L/\overline{v}\,, \tag{6.1}$$

$$P_e = vr_L/D = r_L/\alpha\,, \tag{6.2}$$

$$A = \frac{\phi_m}{b}\sqrt{R_m D_m}\,, \tag{6.3}$$

$$R_\phi = \frac{\phi_m}{\phi_f}\left(1-\phi_f\right), \tag{6.4}$$

where $Ai()$ is the Airy function, r_{wL} $(=r_w/r_L)$ is the ratio of the radius (r_w) of the pumping well to the separation (r_L) between injection and pumping wells, s is the Laplace variable, $\overline{v}$ is the mean pore velocity, α is the longitudinal dispersivity, ϕ_f $(=b/B)$ is the fracture porosity, T_0 is the mean residence time of water, P_e is the Peclet number, A is the diffusive mass-transfer parameter, and R_ϕ is the approximate ratio of matrix porosity to fracture porosity.

The analytic solution in the Laplace domain, Equation (4), can be inversely transformed numerically. We employed a numerical method developed by *de Hoog et al.* [1982] and extensively used for field tracer test analysis [e.g., *Moench*, 1991, 1995;

Novakowski, 1992; *Becker and Charbeneau*, 2000]. Through the numerical inversion of Equation (4), the tracer concentration in fractures was calculated for a given transport-parameter set (T_0, P_e, A, and R_ϕ) and other physical parameters. For short-term field tracer tests, tracer mass does not penetrate deeply into the rock matrix, so the observed tracer breakthrough curves are not sensitive to the fourth parameter R_ϕ. Consequently, only the first three parameters need to be calibrated for many tracer tests.

For a weak-dipole test, a fraction of pumped water (containing tracer mass) is reinjected into the injection well. For a pure-dipole test, the injection rate and pumping rate are identical, and 100% the pumped water (containing tracer mass) is reinjected into the injection well after the injection of the initial tracer-mass solution is complete. For these tracer tests, the flow configuration is no longer radially symmetric. The reinjection of pumped water can be accounted for [*Reimus et al*., 2003b]:

$$\overline{C}_{fR}(s) = \frac{\overline{C}_f(s)}{1-\omega\overline{C}_f(s)}, \tag{7}$$

where $\overline{C}_{fR}(s)$ is the analytic solution in the Laplace domain with tracer recirculation, $\overline{C}_f(s)$ is the analytic solution without recirculation, and ω is the recirculation ratio ($\omega = 1$ for pure dipole).

2.2. Tracer Transport Model in Linear Flow

To analyze field tracer tests in linear flow, we used the analytic solution of *Maloszewski and Zuber* [1985, 1990, 1993]. The tracer transport equation in fractures under the linear flow condition can be written as follows:

$$\frac{\partial c_f}{\partial t} + \frac{v}{R_f}\frac{\partial c_f}{\partial y} - \frac{1}{R_f}\frac{\partial}{\partial y}\left(D\frac{\partial c_f}{\partial y}\right) - \frac{\phi_m D_m}{bR_f}\frac{\partial c_m}{\partial x}\Big|_{x=b} = 0, \tag{8}$$

where y is the Cartesian coordinate along the flow direction parallel to fractures. The boundary condition at the injection well changes from the step-function condition, Equation (3.2), to an instantaneous injection condition:

$$c_f(0,t) = \frac{M}{Q}\delta(t), \tag{9}$$

where $\delta(t)$ is the Dirac delta function. The corresponding analytic solution [*Maloszewski and Zuber*, 1985] is given as:

$$c_f(t) = \frac{2M}{\pi^{3/2} Q} \exp\left(\frac{P_e}{2}\right) \int_w^\infty \exp\left[-\xi^2 - \left(\frac{P_e}{4\xi}\right)^2\right] \int_0^\infty \eta \exp(-\varepsilon_1) \cos(\varepsilon_2)\, d\eta\, d\xi\,, \tag{10}$$

where

$$w = 0.5\left(\frac{P_e T_0}{t}\right)^{1/2} \tag{11.1}$$

$$\varepsilon_1 = \frac{P_e T_0 A}{8} \frac{\eta}{\xi^2} \frac{\sinh(\varsigma) - \sin(\varsigma)}{\cosh(\varsigma) + \cos(\varsigma)} \tag{11.2}$$

$$\varepsilon_2 = \frac{\eta^2}{2}\left(t - 0.25 P_e \frac{T_0}{\xi^2}\right) - \frac{P_e T_0 A}{8} \frac{\eta}{\xi^2} \frac{\sinh(\varsigma) + \sin(\varsigma)}{\cosh(\varsigma) + \cos(\varsigma)} \tag{11.3}$$

$$\varsigma = \frac{R_m R_\phi}{A} \eta \tag{11.4}$$

and ξ, and η are two integration (dummy) variables. Note that for a given set of transport parameters (T_0, P_e, A, and R_ϕ), the fracture concentration depends only on the time since tracer injection.

When the solution is not sensitive to the parameter R_ϕ, the parallel-fracture model can be approximated by using the single-fracture model [*Maloszewski and Zuber*, 1990]:

$$c_f(t) = \frac{MA}{4\pi Q} \left(P_e R_f T_0\right)^{1/2} \int_0^t \exp\left[-\frac{P_e (R_f T_0 - \eta)^2}{4\eta R_f T_0} - \frac{A^2 \eta^2}{4(t-\eta)}\right] \frac{d\eta}{\left(\eta (t-\eta)^3\right)^{1/2}}. \tag{12}$$

2.3. Reanalysis of a Field Tracer Test

The analytic solutions (models) presented in Sections 2.1 and 2.2 were used for reanalyzing field tracer tests that have no reported D_m^e values. In the reanalysis of each tracer test, the transport-parameter set (T_0, P_e, A, and R_ϕ) was calibrated against the observed breakthrough curve(s). For the calibration, the inverse modeling package for parameter estimation and sensitivity analysis [*Finsterle*, 1999; *Zhou et al*., 2004] was used.

Note that these analytic solutions are valid only for a simplified fracture-matrix system with (1) parallel fractures of identical spacing, (2) constant fracture aperture, (3) constant fluid velocity (for linear flow), (4) constant dispersivity, and (5) constant matrix diffusion coefficient. In this case, T_0 (residence time) represents uniform advection, P_e

represents the local-scale mechanical dispersion, and A represents the diffusive mass transfer between fractures and the rock matrix.

When the analytic solutions are used to calibrate a field tracer test, the calibrated transport parameters incorporate additional transport mechanisms not considered in the idealized transport models, and thus are effective parameters. Under natural field conditions, the calibrated T_0 represents the mean residence time for different flow channels caused by aperture variability in single fractures and by different fractures in fracture networks. The calibrated P_e parameter represents the dispersion and spreading caused by the difference in velocity within and between different flow channels. The calibrated A parameter (as well as mean fracture aperture and mean matrix porosity) can be used to calculate the field-scale matrix diffusion coefficient based on Equation (6.3). (The additional transport mechanisms represented by the effective matrix diffusion coefficient will be discussed below in Section 4.1.) Note that in this study, the effective (*field-scale*) matrix diffusion coefficient is used to differentiate it from the (*lab-scale*) matrix diffusion coefficient measured at the lab-core scale, while the other calibrated parameters (T_0 and P_e) (and resulting dispersivity) are automatically referred to as effective parameters for field conditions.

To investigate the scale dependence of the effective matrix diffusion coefficient, we employ the effective-matrix-diffusion-coefficient factor, F_D, which is defined as the ratio of effective matrix diffusion coefficient to the lab-scale matrix diffusion coefficient (D_m):

$$F_D = \frac{D_m^e}{D_m}. \tag{13}$$

The lab-scale matrix diffusion coefficient (D_m) used in Equation (13) is the mean value of laboratory measurements for small rock-matrix samples from the same geologic site. When such measurements are not available, Archie's law [*Boving and Grathwohl*, 2001] is used to approximate this value, based on

$$D_m = \phi_m^{n-1} D_w \ , \tag{14}$$

where D_w is the molecular diffusion coefficient of a tracer in free water, and n is an empirical parameter, which is generally larger than 2.0. To avoid potential exaggeration of scale effects (or an artificial increase in estimated F_D values), we used $n = 2$ here. Unlike the effective matrix diffusion coefficient, F_D is expected to be independent of individual tracers used in field tests, but would depend on the scaling effects of fractured

rock characteristics. In the following sections, the effective matrix diffusion coefficient and its factor are calculated for each tracer test.

3. Field Data on Effective Matrix Diffusion Coefficient

Field observations from about 40 different fractured geologic sites (including results from field tracer tests conducted in different flow configurations and from naturally occurring isotopic tracer migration and contaminant transport events) were first collected from the literature. These observations were then used for generating a data set of effective matrix diffusion coefficients.

3.1. Field Tracer Tests and Observations

A number of field tracer tests were conducted in fractured rock in the 1970s and 1980s [e.g., *Webster et al*., 1970; *Lenda and Zuber*, 1970; *Grove and Beetem*, 1971; *Kreft et al*., 1974; *Claassen and Cordes*, 1975; *Ivanovich and Smith*, 1978; *Gustafsson and Klockars*, 1981; *Tester et al*., 1982; *Black and Kipp*, 1983; *McCable et al*., 1983; *Cullen et al*., 1985; *Garnier et al.*, 1985; *Novakowski et al*., 1985; *Raven et al.*, 1988; *Shapiro and Nicholas*, 1989]. These tests were conducted to estimate rock properties (e.g., fracture porosity and dispersivity) for groundwater flow and transport in fractured media for (1) nuclear waste disposal [*Webster et al*., 1970; *Davison et al*., 1982; *Novakowski et al*., 1985; *Raven et al.*, 1988], (2) aquifer water resources [e.g., *Black and Kipp*, 1983], (3) geothermal reservoir production [e.g., *Tester et al*., 1982; *Horne and Rodriguez*, 1983; *McCable et al*., 1983], and others. The original analyses of these tests were based on advection-dispersion models, neglecting the effects of matrix diffusion [e.g., *Zuber*, 1974; *Robinson and Tester*, 1984; *Shapiro and Nicholas*, 1989]. Some of these tests were reanalyzed and reported in the literature by using analytic models with matrix diffusion, which are the same as or similar to the analytic models discussed in Sections 2.1 and 2.2 [*Hodgkinson and Lever*, 1983; *Maloszewski and Zuber*, 1985, 1990, 1992, 1993; *Bullivant and O'Sullivan*, 1989; *Moench*, 1995]. The reported field-scale matrix-diffusion-coefficient values were used directly as entries to our data set. Of the remaining tracer tests (without reported D_m^e values), some were selected based on data availability and quality (to be discussed in the following section) and reanalyzed to obtain the corresponding D_m^e values.

Since 1990, a large number of field tests have been conducted using conservative nonsorbing and reactive sorbing tracers in natural-gradient flow [*Himmelsbach et al*., 1998; *Jardine et al*., 1999; *Lapcevic et al*., 1999; *Maloszewski et al*., 1999], induced linear flow (e.g., by infiltration) [*Cacas et al*., 1990b; *Abelin et al*., 1991a, b; *Birgersson et al*., 1993; *McKay et al*., 1993a; *Sidle et al*., 1998; *Salve et al*., 2004], induced

convergent or weak-dipole flow [*Jones et al*., 1992; *Cady et al*., 1993; *Hadermann and Heer*, 1996; *D'Alessandro et al*., 1997; *Garcia Gutierrez et al*., 1997; *Gylling et al*., 1998; *Himmelsbach et al*., 1998; *Hoehn et al*., 1998; *Becker and Shapiro*, 2000; *Karasaki et al*., 2000; *Meigs and Beauheim*, 2001; *Widestrand et al*., 2001; *Baumle*, 2003; *Lee et al*., 2003; *Reimus et al*., 2003a, b; *Andersson et al*., 2004; *Brouyere et al*., 2004], induced divergent flow [*Novakowski*, 1992; *Novakowski and Lapcevic*, 1994], induced dipole recirculating flow [*Frost et al*., 1992, 1995; *Scheier et al*., 1993; *Jakoben et al*., 1993; *Sawada et al*., 2000], induced single-well divergent-convergent flow [*Meigs and Beauheim*, 2001; *Becker and Shapiro*, 2003], and in complicated flow (varying between tracer source to observation points) [*Gustafsson and Andersson*, 1991]. Many of these tests were conducted using multiple tracers [e.g., *Reimus et al*., 2003a, b], multiple flow rates [e.g., *Becker and Shapiro*, 2000], and multiple flow configurations [e.g., *Frost et al*., 1995] to reduce the uncertainties (e.g., nonuniqueness) in calibrated transport parameters. In addition, the bacteriophage and microsphere have been injected simultaneously or separately with chemical tracers to separate the effects of matrix diffusion from advection and dispersion [*Champ and Schroeter*, 1988; *Bales et al*., 1989; *McKay et al*., 1993b; *Becker et al*., 1999; *Reimus and Haga*, 1999]. At some geologic sites, tracer tests have been conducted at different scales to investigate scale effects of transport parameters [*Novakowski and Lapcevic*, 1994; *Frost et al*., 1995; *Himmelsbach et al*., 1998; *Jardine et al*., 1999; *Maloszewski et al*., 1999; *Baumle*, 2003]. Of all the field tracer tests, most have been analyzed using analytic or numerical models considering matrix diffusion [e.g., *Brettmann et al*., 1993], and their reported values of field-scale matrix diffusion coefficients were again used as entries to our data set. Some of the remaining tracer tests with this coefficient (D_m^e) unavailable were reanalyzed to obtain the corresponding D_m^e values.

In addition to field tracer tests, a few long-term, large-scale isotopic tracer and contaminant transport events in regional groundwater flow in fractured rock have been observed [e.g., *Bibby*, 1981; *Pankow et al.*, 1986; *Johnson et al*., 1989; *Rudolph et al*., 1991; *Shapiro*, 2001]. These large-scale observations are essential to our investigation of the field-scale matrix diffusion coefficient over a larger range of observation scales, because all field tracer tests were conducted at scales less than 1,000 m.

3.2. Criteria for Tracer-Test Selection

Of the collected field observations from about 40 fractured geologic sites, only a fraction were selected to examine the scale-dependence of the effective matrix diffusion coefficient. Four major criteria were used for selecting the tracer tests used in this study.

First, the selected tracer tests must be conducted in fractured rock with a significant contrast between fracture and matrix permeability. Tracer tests conducted in other fractured porous media were not considered here. Examples of these fractured porous media are fractured tills immediately under the ground surface [*McKay et al*., 1993a, b; *Sidle et al*., 1999] and fractured permeable media with small permeability contrast (i.e., one or two orders of magnitude) and very small fracture length [*Jones et al*., 1992; *Ostensen*, 1998; *Meigs and Beauheim*, 2001]. This criterion is based on a consideration that in fractured rock, diffusive mass transfer dominates the mass exchange at the fracture-matrix interface, and the estimated effective matrix diffusion coefficient is representative of the dominant diffusion process. However, in a fractured porous medium (with small permeability contrast), advective and dispersive mass transfer may exist between fractures and the matrix, and it is difficult to distinguish the advective-dispersive mass transfer from diffusive mass transfer at the fracture-matrix interface. On the other hand, solute transport in fractured media with very small fracture length (on the order of centimeters) may be similar to that in porous media, but is not typical for fractured rock, which is of interest here.

Second, the tracers used in the selected tests must be conservative. For nonconservative tracers, one or more additional parameters are needed to account for the corresponding adsorptive, reactive, or radioactive decay processes, complicating the transport-parameter calibration. In most cases, field tests of nonconservative tracers are usually conducted simultaneously with (or after) conservative tracer tests [e.g., *Andersson et al*., 2004]. In practice, the conservative tracer tests are often used to determine the transport parameter set (T_0, P_e, A) for advection, dispersion, and matrix diffusion, and the nonconservative tracer tests are used to determine the additional parameters. In many tracer tests, multiple tracers of different molecular-diffusion-coefficient values are used to confirm the presence of matrix diffusion and to reduce the uncertainties involved in the calibration of transport parameters.

Third, a selected tracer test must be well defined, with clear breakthrough curves and detailed information on the tracer tests (e.g., injection mass, injection and pumping rates). These data are critical for accurate calibration of the transport parameters using the analytic models. A number of field tracer tests did not have detailed testing data documented in the literature [e.g., *Claassen and Cordes*, 1975; *Cullen et al*., 1985], and some other tracer tests were terminated too early without the tailing limb recorded [e.g., *Grove and Beetem*, 1971]. For example, many tracer tests in the 1970s were conducted to estimate fracture (advective) porosity and dispersivity by recording the rising limb only of breakthrough curves [e.g., *Grove and Beetem*, 1971]. There also were some field tests in the literature conducted under natural-gradient-flow conditions, and with too low a

mass recovery [*Tester et al*., 1982; *McCabe et al*., 1983]. Under these circumstances, it is impossible to accurately estimate the field-scale matrix diffusion coefficient.

Finally, fracture aperture and matrix porosity must be available for calculating the effective matrix diffusion coefficient (with the calibrated A parameter). In many cases, however, the fracture aperture (independently determined from direct measurements, or from calculations using hydraulic or tracer tests) or matrix porosity (measured from matrix cores) was not available, because no detailed site characterization had been conducted for the given geologic sites.

3.3. Summary of Observations

A literature survey was conducted to compile effective matrix-diffusion-coefficient values obtained from field-scale tracer tests and their analysis. The literature sources and pertinent data characterizing each of the surveyed sites are summarized in Table 1. Blank entries in the table indicate that the information was not available from the literature. This table summarizes information for purposes of comparison only. The details of a particular geologic site may be found in the original reference sources.

Fractured rock characteristics. As indicated by the fourth-through-eighth columns in Table 1 (from the left), the study sites represent a wide variety of fractured media and settings. Summarized in these columns is information on fractured materials, average thickness of the fracture zone or single fracture, mean matrix porosity, measured (or calculated) fracture aperture, and hydraulic conductivity or transmissivity. Fractured rock materials include granitic rock with small matrix porosity, fractured shale with medium matrix porosity, and fractured chalk with large matrix porosity. The thickness effective for a tracer test depends on whether the tracer tests are conducted within a single fracture or a fracture zone. In several tracer tests conducted in a single fracture, the thickness is the fracture aperture, ranging from 0.06 to 2.9 mm. For the other tests, tracer moves through a fracture zone with a number of fractures, and the thickness is the arithmetic average of the screen length of pumping and injection wells. In this case, the thickness ranges from 0.64 to 76 m. Matrix porosity is usually measured from intact rock-matrix cores. The matrix porosity in Table 1 ranges from 0.3% for granitic rock to 40% for chalk; for a given geologic site, the relative variability in matrix porosity may not be high. For example, the matrix porosity for the British Chalk ranges from 0.15 to 0.40, with the ratio (of maximum value to minimum value) less than 3. Fracture aperture is usually measured for a single fracture in the field, or calculated using the fracture porosity and the fracture spacing measured from fracture surveys of a fracture zone [*Maloszewski and Zuber*, 1993]. Fracture aperture can also be calibrated using hydraulic tests with drawdown or estimated roughly from fracture permeability and porosity [*Maloszewski and Zuber*, 1993, Equation 17].

Tracer test characteristics. The ninth-through-eleventh columns in Table 1 summarize the features of the tracer tests in determining transport parameters for each site. Summarized in these columns is information on flow configuration, injection and pumping flow rates, tracer type, and tracer injection mass. Flow configuration in Table 1 includes convergent, weak dipole, pure dipole (two-well recirculating), and natural-gradient flow. Controlled tracer tests may be conducted under ambient groundwater flow conditions (here referred to as "natural-gradient tests") or under conditions in which the flow configuration is induced by pumping or injection. In a convergent flow field, the tracer is injected in an injection well, and the corresponding breakthrough of tracer concentration is recorded in a distant pumping well. The injection flow rate for the tracer-mass injection period is negligible. In a convergent-flow tracer test, a fraction of the injected tracer mass may stay within the injection borehole and does not contribute to the breakthrough curve at the pumping well. In a weak-dipole tracer test, both an injection well and a pumping well are operating at different flow rates for the entire testing period. After the tracer-mass injection is complete, a small fraction (say 5%) of the pumped water (containing tracer) from the pumping well is re-injected into the injection well to flush the tracer mass remaining within the injection boreholes and to reduce the borehole storage effects. The pumping and injection flow rates remain unchanged through the entire tracer test. The pure-dipole tracer test is different from a weak-dipole test only in that in the former, 100% of the pumped water is recirculated to the injection well, and the pumping and injection flow rates are identical. At some geologic sites, different tracer tests in different flow configurations have been conducted [*Frost et al*., 1995; *Becker and Shapiro*, 2000].

Different flow rates between the injection and pumping wells at the same site were used in some tracer tests. In the multi-flow-rate test, the identical dispersivity and matrix diffusion coefficient is expected for different tests with different flow rates, and the mean residence time varies with the flow rates. All the breakthrough curves obtained in the multi-flow-rate test (which is a set of tracer tests) were calibrated simultaneously to reduce the uncertainties and non-uniqueness of the calibration.

Fitting the transport-parameter set. The twelfth-through-fourteenth columns in Table 1 summarize the fitted transport parameters: the mean residence time (T_0), the Peclet number (P_e), and the mass-transfer parameter (A). In most cases, the porosity ratio R_ϕ is insensitive to measured breakthrough curves (because the tracer mass was away from the central line between neighboring fractures during the entire tracer tests) and thus the single-fracture approximation (corresponding to the infinite fracture spacing) can be used. For a tracer test with reported tracer-test analysis in the literature (using the two tracer-transport models above or similar models), we listed directly the reported

values for the transport parameter set. For the other tracer tests listed in Table 1, reanalysis was conducted to calibrate the transport-parameter set against the measured tracer breakthrough curves.

Effective matrix diffusion coefficient and observation scale. The fifteenth-through-eighteenth columns in Table 1 summarize the effective matrix diffusion coefficient (D_m^e), lab-scale matrix diffusion coefficient (D_m), observation scale (L or r_L), and the effective-matrix-diffusion-coefficient factor (F_D). The D_m^e value is calculated based on the reported (or reanalyzed) value of the mass-transfer A parameter, fracture aperture, and matrix porosity available in the literature. The lab-scale matrix diffusion coefficient is often obtained from laboratory "through-diffusion" experiments on rock-matrix cores for a given conservative tracer, and a mean lab-scale value can be calculated from measurements of different intact rock-matrix cores for a given site.

The effective-matrix-diffusion-coefficient factor ($F_D = D_m^e / D_m$) is calculated using the effective and lab-scale matrix diffusion coefficients, and is expected to be independent of the tracers used. The observation scale is the separation between the injection and pumping wells in a radial flow configuration, or the distance between the tracer source point and the sampling location in a natural-gradient flow condition.

4. Results and Discussion

Table 1 lists 40 values of the effective matrix diffusion coefficient from 15 fractured sites, obtained through calculations of the mass-transfer parameter A reported in the literature and reanalyzed in this study. The effective-matrix-diffusion-coefficient factor (F_D) is calculated for each of these effective matrix diffusion coefficients. Figure 1 shows the data on the effective-matrix-diffusion-coefficient factor, as a function of the observation (test) scale.

4.1. Enhancement and Scale Dependence of the Effective Matrix Diffusion Coefficient

As shown in Table 1, the effective-matrix-diffusion-coefficient factor is generally larger than one, indicating that the matrix diffusion coefficient at the field scale is enhanced in comparison with the corresponding value at the lab-core scale. The enhancement of field-scale effective matrix diffusion coefficient is different for different types of fractured rock. For granitic rock with small matrix porosity, the field-scale matrix diffusion coefficient is significantly larger than its corresponding lab-scale value, as indicated by the large F_D value. Although the lab-scale matrix diffusion coefficient is

usually small for granite, the field-scale matrix diffusion coefficient is relatively large for most of the field tracer tests conducted in fractured granitic rock. (The large number of data points available for granitic rock possibly results from the drive to store nuclear waste in deep saturated granitic rock in many countries.) As a result, matrix-diffusion enhancement cannot be neglected in analyzing a field tracer test conducted in a fractured granitic rock merely because of the common very small lab-scale value.

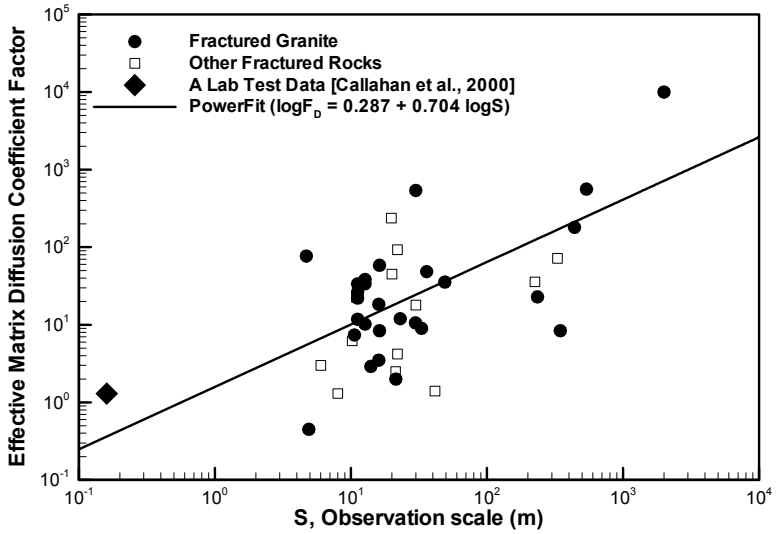

Figure 1. Effective matrix diffusion coefficient factor for different fractured rocks, as a function of observation scale

As shown in Figure 1, the general trend is for the effective-matrix-diffusion-coefficient factor (F_D) to increase with observation scale. The F_D value varies from 1 to 10,000 for the observation scale from 5 m to 2,000 m. A moderate slope is obtained for the effective-matrix-diffusion-coefficient factor as a function of observation scale. In addition, two clusters of data points of the effective-matrix-diffusion-coefficient factor and observation scale can be distinguished, because few data points are available in between the two scale clusters. Most field tracer tests are conducted at a small scale ($5 < L < 50$ m) in the first cluster. In the second cluster, there are seven data points for the scale over 100 m. The maximum observation scale for environmental tracers is about 2,000 m in a fractured crystalline rock [*Shapiro*, 2001], whereas the maximum scale for field tracer tests is 538 m in an inclined fractured granitic rock zone [*Webster et al.*, 1970]. As can be seen, the over-hundred-meter-scale observations are critical for the effective matrix-diffusion-coefficient extrapolation to a larger scale.

For a given scale, the F_D value varies over two orders of magnitude. This is particularly true for the small-scale observations in the first cluster, because there are sufficient data points to characterize this variability, whereas only a few data points are available to define this variability for the over-hundred-meter-scale observations in the second cluster. The variability in the F_D value for a given scale may be related to the type of fractured rock (granite, chalk, or tuff), heterogeneity of the fracture network, and to the heterogeneity of the matrix rock along single fractures.

The mechanisms involved in causing the potential scale dependence of the effective matrix diffusion coefficient and their relative importance are not clear. However, the observed enhancement of field-scale matrix diffusion may be attributed to complicated mass-transfer processes in a naturally heterogeneous fractured rock system. This is because the calibrated mass-transfer parameter A and the effective matrix diffusion coefficient represent these processes at different scales (as well as the diffusion process within the rock matrix).

These complicated diffusive mass-transfer processes require further discussion. The rock matrix may be highly heterogeneous (in porosity and diffusion coefficient) with the penetration depth into the matrix from fractures. An altered and degraded zone with relatively high matrix porosity may exist between fractures and the intact rock matrix [*Zhou et al*., 2005]. This so-called degraded zone may result from the variable degree of chemical alteration and recrystallination and a high frequency of microfractures caused by deformation due to tectonic forces [*Andersson et al*., 2004, Figure 3]. The degraded zone may vary in its thickness and porosity in space, resulting in irregular matrix diffusion into the rock matrix. This degraded zone may be a layer of fracture coating [*Skagius and Neretnieks*, 1986] or a layer of karstic rock [*Maloszewski and Zuber*, 1993]. The matrix porosity in the degraded zone (higher than that in the intact rock matrix) may contribute to the enhancement of field-scale matrix diffusion [*Hodgkinson and Lever*, 1983; *Maloszewski and Zuber*, 1993; *Andersson et al*., 2004]. In addition, infilling materials and fault gouge materials may be found within fractures. These materials are often unconsolidated materials consisting of altered wall rock fragments infilled with clays [*Maloszewski and Zuber*, 1993; *Andersson et al*., 2004]. The degraded zone and infilling materials have been identified by surveying natural fractures and their surrounding rock [*Andersson et al*., 2004], and by different diffusion processes exhibited in observed breakthrough curves in field tracer tests in a single fracture [*Zhou et al*., 2005].

A natural fracture usually exhibits variability in its aperture [e.g., *Brown and Scholz*, 1985; *Tsang et al*., 1991; *Novakowski and Lapcevic*, 1994]. Field- and laboratory-scale experiments and theoretical investigations strongly suggest that aperture variability

may result in flow focusing and channeling in a single fracture plane [e.g., *Tsang et al*., 1988; *Moreno et al*., 1988]. Based on the cubic law for fracture permeability, flow channels occur in the regions with large aperture, leaving the remaining regions with little or no global flow. The so-called large-aperture regions may occupy less than 20% of the entire fracture plane area, resulting in a smaller effective interface area for diffusive mass transfer between fractures and the matrix. On the other hand, the so-called large-aperture regions may be in contact with small-aperture ones, and diffusive mass transfer may occur between flowing water in the former (of a single fracture) and stagnant water in the latter [e.g., *Johns and Roberts*, 1991; *Neretnieks*, 2002]. The solute mass diffused into the small-aperture regions from large-aperture ones may further diffuse into the rock matrix in contact with the small-aperture regions. In the case that the aqueous diffusion coefficient is much larger than the matrix diffusion coefficient (e.g., in fractured granite), the diffusive mass transfer between flowing and stagnant water within fractures may be dominant in comparison with the mass transfer between flowing water in channels and stagnant water in the rock matrix [*Johns and Roberts*, 1991]. As a result, the matrix diffusion coefficient is enhanced by the additional diffusive mass transfer within fractures (in comparison with fracture-matrix diffusion), and the effective matrix diffusion coefficient calibrated using field tracer tests may represent this kind of enhancement.

Fractures exist at different scales. Within a fracture network, the global flow may carry solutes through only a fraction of connected fractures (back bones), leaving the remaining connected fractures bypassed by global flow [e.g., *Rasmuson and Neretnieks*, 1986]. These bypassed fractures may, however, contribute to global transport by diffusive mass transfer between themselves and channels of global flow. In addition, there may be pervasive so-called small-scale fractures [*Wu et al*., 2004] usually neglected in field surveys, data processing (e.g., for fracture density and frequency), and modeling assessment. These small fractures may not contribute to the global flow, but they do contribute to global transport by presenting additional paths for mass transfer between fractures and the matrix. The possible highly important effects of the small fractures have been confirmed by *Wu et al.* [2004], who developed a triple-continuum model consisting of the matrix, locally connected small-scale fractures, and globally connected large fractures. Therefore, field-scale matrix diffusion may also be enhanced by the mass transfer between global-flow fractures, bypassed fractures, small fractures, and ultra-small fractures.

Some of the mechanisms for the enhancements discussed above may be related to the scale dependence of the effective matrix diffusion coefficient. *Liu et al*. [2004b] attempted to use a fractal concept to explain both the enhancement and the scale-dependence of the effective matrix diffusion coefficient. The fractal concept has been found to be useful for describing both subsurface heterogeneity and many flow and

transport processes [e.g., *Wheatcraft and Tyler*, 1988; *Molz and Boman*, 1993]. In commonly used numerical and analytic models of solute transport, including matrix diffusion, an actual fracture network is generally conceptualized as parallel vertical or horizontal fractures, and a fracture wall is approximated as a flat wall. In this case, solute-particle travel paths within fractures are generally straight lines. However, the actual solute-particle travel path is much more intricate and tortuous, for the following reasons. First, fracture walls are not flat but rough. The rough surface generates a much larger fracture-matrix interface area than a flat fracture wall, and the fracture roughness is characterized by fractals [*National Research Council*, 1996, *Molz et al*., 2004]. Second, fractures exist at different scales, with small-scale fractures generally excluded from modeling studies [*Wu et al*., 2004]. However, the existence of fractures at different scales can make flow and transport paths much more tortuous than straight lines. Considering that both fracture roughness and fracture-network geometry can be characterized by fractals [e.g., *Barton and Larsen*, 1985; *Molz et al*., 2004], *Liu et al.* [2004b] hypothesize that a solute travel path within a fracture network is fractal, rather than a straight line (as assumed in many numerical or analytic models). This fractal behavior may result in the scale dependence of a fracture-matrix interface area along a solute transport path, and therefore may result in the scale dependence of the effective matrix diffusion coefficient (related to the interface area).

The heterogeneity of the intact rock-matrix properties may also play a role in determining the effective matrix diffusion coefficient. The lab-scale matrix diffusion coefficient used in Table 1 is the mean value of core-scale matrix-diffusion-coefficient values measured for a number of rock-matrix cores sampled from the same geologic site. In the case with the core-scale value unavailable, the mean matrix porosity is used to calculate the lab-scale matrix diffusion coefficient using Equation (14). The core-scale matrix diffusion coefficient is usually measured by through-diffusion experiments on a core of rock matrix under laboratory conditions [e.g., *Callahan et al*., 2000]. It represents the lumped matrix diffusion coefficient for the core as a whole. Within the core, the matrix diffusion coefficient may vary with heterogeneous porosity and formation factors, as evidenced by imaging techniques [e.g., *Tidwell et al*., 2000; *Altman et al*., 2004]. The lab-scale matrix diffusion coefficient may also vary with different cores. The inner-core and core-to-core variability may introduce uncertainties in the calculated F_D value. However. the mean lab-scale matrix diffusion coefficients used in this study are considered to be representative for the given geologic sites [e.g., *Birgersson and Neretnieks*, 1990; *Fleming and Haggerty*, 2001].

Related to the local-scale heterogeneity of diffusive properties, *Haggerty and Gorelick* [1995] developed a multirate diffusion model to consider this heterogeneity. This model was successfully applied to fractured dolomite with small permeability

contrast between fractures and the matrix [*Fleming and Haggerty*, 2001; *Haggerty et al*., 2001; *McKenna et al.*, 2001]. Recently, *Haggerty et al*. [2003] indicated the temporal-scale dependence of mass-transfer coefficient for porous and fractured media, as a signature of the multirate diffusion processes, by compiling a larger number of test results. They showed that the mass-transfer coefficient decreased with testing time for porous-medium results, but the trend was not obvious for fractured media (see their Figure 1). Their mass-transfer coefficient was conceptually similar to the effective matrix diffusion coefficient here. However, we do not observe the temporal-scale dependence for fractured rock at the selected geologic sites, as indicated in Figure 2a. This may result from the fundamental differences between heterogeneous pore structures in porous media and complex fracture geometry (and its interaction with porous rock matrix) in fractured rock. An alternative explanation is that most mass-transfer coefficients presented in *Haggerty et al*. [2003] were obtained using first-order mass-transfer models. These models generally overestimate the mass-transfer coefficient at early experiment periods, because of the existence of the sharp concentration gradient at the interface between mobile and immobile zones. In our analysis, however, the time-dependent concentration gradients at the fracture-matrix interface and the mass transfer from fractures to the matrix are captured analytically and exactly; as a result, the overestimation is not an issue here.

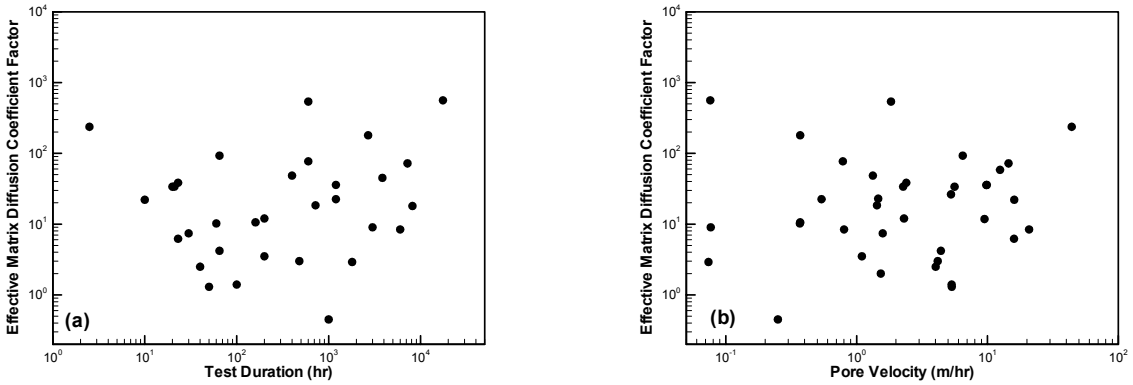

Figure 2. Effective matrix diffusion coefficient factor, as a function of (a) the duration of tracer tests and (b) mean pore velocity of water

Shapiro [2001] showed that to match tracer data observed at a kilometer scale, a matrix diffusion coefficient three to five orders of magnitude greater than that from laboratory experiments was needed. This result is included in Figure 1. His analysis probably provides the first estimate for a kilometer-scale effective matrix diffusion

coefficient in the literature. He also suggested that kilometer-scale effective matrix diffusion is not a true diffusive process, but actually an advective process between high- and low-permeability zones, resulting in a very large effective matrix diffusion coefficient. His argument is based mainly on studies of solute transport in heterogeneous porous media [*Shapiro*, 2001]. If the argument is valid, one would expect to see a correlation between the effective matrix diffusion coefficient and pore velocity [*Haggerty et al*., 2003]. Indeed, as demonstrated by *Bajracharya and Barry* [1997] and many others, the effective mass-transfer coefficient for a heterogeneous porous medium (conceptually similar to the effective matrix diffusion coefficient for fractured rock) increases with pore velocity. (More discussion of this correlation can be found in *Bajracharya and Barry* [1997] and *Haggerty et al*. [2003].) However, we do not observe a meaningful correlation between the effective matrix diffusion coefficient and pore velocity, as indicated in Figure 2b. The lack of correlation was also obtained by *Haggerty et al.* [2003] after analyzing a substantial number of test results for porous and fractured media. Therefore, the use of advective mass-transfer mechanism to interpret for enhancing the effective matrix diffusion coefficient in fractured rock may need further examination.

In summary, a number of complicated mass transfer processes may result in the enhancement of the effective matrix diffusion coefficient. These processes may contribute to the scale dependence observed in this study. Identifying and searching for the dominant mechanisms for this scale dependence will be a topic of our future research.

4.2. Scale-Dependence of Field-Scale Dispersivity

In addition to the effective matrix diffusion coefficient, we also collected or estimated longitudinal dispersivity values for different tracer tests. To evaluate the reasonableness of our calibrated transport parameters, we checked the consistency of the dispersivity data in this study with past studies of calibrated dispersivity versus scale.

As shown in Figure 3, the longitudinal dispersivity, in general, depends on observation scale. The field-scale dispersivity varies from 0.1 m to 250 m for a range of observation scales between 5 and 2,000 m. For the meters-scale tracer tests, the dispersivity is less than 1.0 m; for the tens-meter-scale tracer tests, the field-scale dispersivity is less than 10 m; for the hundreds-meter-scale tracer tests, the dispersivity is larger than 2.0, but less than 50 m. The maximum dispersivity value of 250 m corresponds to the maximum scale of 2,000 m [*Shapiro*, 2001], while the minimum dispersivity value of 0.1 is obtained for the multi-tracer test conducted in fractured shale bedrock [*Jardine et al*., 1999]. For the tens-meter scale, sufficient dispersivity values are available to address the dispersivity variability for a given scale. The one-order-of-magnitude variability may represent different degrees of heterogeneity in fractured rock.

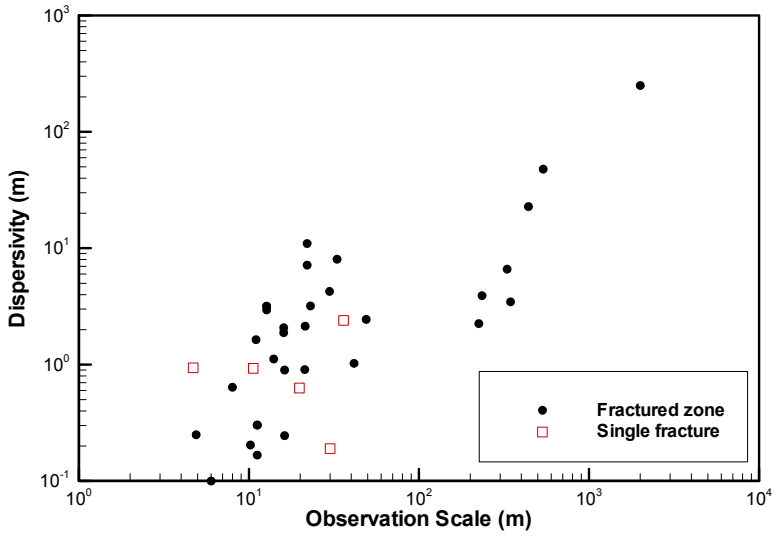

Figure 3. Field-scale longitudinal dispersivity in fractured rock as a function of observation scale

Shown in Figure 4 is a comparison of our data set to that data set from Table 1 in *Gelhar et al*. [1992], who compiled dispersivity data for examining scale-dependent behavior in both porous and fractured media. Our data are consistent with their data over a larger range of observation scales. Their data were gathered from both field tracer tests and environmental-tracer-migration observations in fractured and porous media, over a scale ranging from 0.75 to 100,000 m, whereas our data set corresponds to the field-scale dispersivity from controlled tracer tests (with one exception) in fractured rock over a smaller range of observation scales between 5.0 and 2,000 m.

It is also useful to compare our data set (for fractured rock) with the data set for fractured media only in *Gelhar et al*. [1992]. First, our data set can be classified as one of high quality, based on their selection criteria for high-quality data points. Only four of their data points for fractured media are included in our investigation, because the others do not meet our tracer-test selection criteria. For example, the data point [*Grove and Beetem*, 1971] in their Figure 1 is not considered in our study, because the recorded breakthrough curve contains the rising limb only—the falling limb is critical to accurately estimating dispersivity by distinguishing the dispersion effect from the matrix diffusion effect. Second, for the same tracer tests, our calibrated dispersivity values are smaller than the corresponding values given in *Gelhar et al*. [1992] (see Figure 4). For example, our calibrated dispersivity for the field tracer test conducted by *Webster et al*. [1970] is

48 m, whereas the value in *Gelhar et al*. [1992] is 134 m. Our dispersivity data are obtained by calibrating against the field tracer tests, using tracer-transport models considering diffusive mass transfer between fractures and the matrix, as well as advection and dispersion in fractures. Their field-scale longitudinal dispersivity values were obtained by analyzing tracer tests using advection-dispersion models only, without consideration of matrix diffusion [*Webster et al*., 1970; *Grove and Beetem*, 1971; *Kreft et al*., 1974; *Claasen and Cordes*, 1975; *Ivanovich and Smith*, 1978]. When the advection-dispersion model is used to calibrate a field tracer test conducted in a fractured rock aquifer with significant matrix diffusion effects, the Peclet number needs to decrease and the residence time needs to increase to match the highly skewed breakthrough curve with long tailing [*Maloszewski and Zuber*, 1985, 1990, 1993; *Moench*, 1995; *Reimus et al*., 2003b]. If this adjustment isn't made, an erroneously large longitudinal dispersivity is produced.

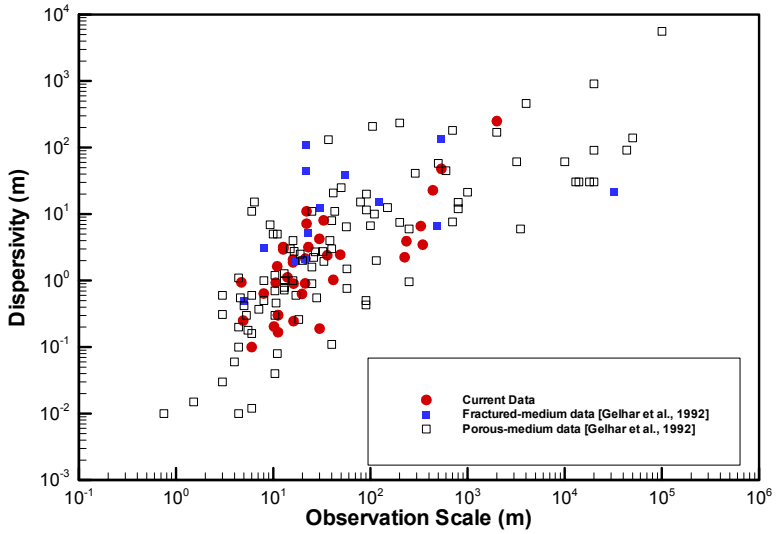

Figure 4. Comparison of the field-scale longitudinal dispersivity between the current study for fractured rock and a previous study for both porous and fracture media [*Gelhar et al.*, 1992]

The calibrated field-scale dispersivity represents the mixing and spreading phenomena (1) across fracture apertures, (2) along fracture planes, and (3) within a fracture network (as well as different flow streamlines under dipole flow conditions [*Grove and Beetem*, 1971]). The first two mixing and spreading processes can be seen in the calibrated dispersivity values from field tracer tests conducted in single-fracture systems. In our data set, there are five tracer tests conducted in a single fracture. The

Peclet number varies from 5.0 to 160, and the dispersivity varies from 0.19 to 2.4 m. Across-fracture-aperture mixing is caused by the non-uniform (parabolic) fluid velocity distribution within the fracture aperture, as well as by molecular diffusion from the high-velocity center to a lower-velocity region adjacent to fracture walls. For a smooth fracture with constant aperture, this mixing can be described by Taylor dispersion [*Taylor*, 1953; *Roux*, 1998; *Detwiler et al*., 2000]. The Taylor dispersion coefficient D_T, and dispersivity, α_T, can be written as:

$$D_T = \frac{1}{210}\frac{v^2(2b)^2}{D_w} \quad \text{and} \quad \alpha_T = \frac{1}{210}\frac{v(2b)^2}{D_w}. \tag{15}$$

As shown in Equation (15), the dispersivity of Taylor dispersion depends only on mean fluid velocity, fracture aperture, and the molecular diffusion coefficient in free water. It is independent of observation scale. This is understandable, because Taylor dispersion describes the local cross-aperture mixing, rather than along the fracture. We calculated the dispersivity values of Taylor dispersion (using the known mean velocity and fracture aperture) for the five single-fracture tracer tests, and compared them with their calibrated field-scale dispersivity values. In all cases except one, the Taylor dispersivity is negligible ($< 1\%$) compared to the field-scale dispersivity. (One exception is the case in *Shapiro and Nicholas* [1989], in which both fracture aperture and velocity are very large, and the resulting Taylor dispersivity is 50% of the calibrated field-scale dispersivity.) Therefore, the field-scale dispersivity must be caused by spatial variability in the velocity distribution along the fracture plane. This spatial variability may result from the variability of fracture aperture, as suggested by both *in situ* borehole observations and lab imaging on fracture samples [e.g., *Novakowski and Lapcevic*, 1994]. Another reason for velocity variability may be the roughness of fracture walls. Consequently, the calibrated P_e parameter and resulting dispersivity is representative of the field-scale mixing phenomena caused by the heterogeneity in fracture aperture and roughness within a single-fracture system.

The third mixing and spreading process is evident in the calibrated dispersivity for the tracer tests conducted in fracture networks. For these tracer tests, the calibrated dispersivity is expected to represent the mixing between different fractures at their intersections or junctions (in addition to the first two mixing processes). The tracer mass through several separated fractures may mix together, leading to more spreading of tracer concentration caused by the heterogeneity between different fractures [*Himmelsbach et al*., 1998]. The scale of the mixing depends on the fracture connectivity and the fracture length. In the case of a small length, the mixing between different fractures may happen at a small scale, whereas in the case of long fractures, the mixing may happen at the

pumping well. In reality, many different-length fractures can intersect with each other, forming a well-connected fracture network. For a large-scale test in a densely fractured rock zone, mixing between different fractures may happen at many different scales.

Note that the calibration of the mass-transfer parameter A (for determining the effective matrix diffusion coefficient) and the Peclet number P_e (for determining the field-scale longitudinal dispersivity) may involve some degree of uncertainty and nonuniqueness—as with all other inverse modeling applications. One major concern involved in the calibration is that both matrix diffusion and dispersion contribute to the mixing and spreading of tracer mass. For example, matrix diffusion usually produces long tailing in the observed breakthrough curves, but dispersion with a small P_e value (e.g., $P_e < 2$) also produces long tailing [e.g., *Maloszewski and Zuber*, 1985, Figure 2]. Given the resulting similarity, it is difficult to distinguish the effects of matrix diffusion from dispersion on the observed breakthrough curves. However, more constraints can be used to reduce the uncertainty of the calibration. For all tracer tests reanalyzed in this study, we used all the available data (measured fracture permeability and matrix porosity, multiple flow rates and multiple tracers, etc.) to constrain the calibration. A very good example is the tracer test in *Lenda and Zuber* [1970], which was calibrated using the single-fracture advection-dispersion model with matrix diffusion by *Maloszewski and Zuber* [1985, Figure 11]. Their calibrated parameters were $T_0 = 28.8$ hr, $P_e = 0.33$, and $A = 0.032$ $s^{-1/2}$, but the simulated breakthrough curve was not sensitive to the parameter values. In our reanalysis of this test, we also used another test [*Kreft et al*., 1974] conducted between the same two wells at the same site with a reduced pumping flow rate (1.4 m^3/min), to constrain our calibration, and obtained a more reasonable parameter set: $T_0 = 5.0$ hr, $P_e = 2.0$, and $A = 4.98 \times 10^{-3}$ $s^{-1/2}$; this parameter set produced good match between simulated and measured breakthrough curves for both tests. In some cases, the mean residence time is available in a field tracer test [*Liu et al*., 2004a], and can be used to significantly improve our confidence in calibration. This is because a large dispersivity value produces a much earlier tracer concentration peak than the mean residence time of water, whereas matrix diffusion produces a concentration peak at a later time than the mean residence time of water. As a whole, we believe that field-scale longitudinal dispersivity was properly accounted for in the analyses of field tracer tests listed in Table 1, a belief supported by the consistency between our results and those in *Gelhar et al*. [1992]). The obtained field-scale matrix diffusion coefficient values are thus shown to be reasonable.

5. Summary and Conclusions

Matrix diffusion is an important process for retarding solute transport in fractured rock, and the matrix diffusion coefficient is a key parameter for describing this process. Previous studies have indicated that the effective-matrix-diffusion-coefficient values obtained from field tracer tests are enhanced compared to the matrix-diffusion-coefficient values at the laboratory core scale, and may increase with test scales.

We conducted a comprehensive literature survey in this study for the field-scale (effective) matrix diffusion coefficient D_m^e in fractured rock. The effective value was obtained through the calibrated mass-transfer parameter, A ($=\frac{\phi_m}{b}\sqrt{D_m^e}$), as well as through available data on fracture aperture ($2b$) and matrix porosity (ϕ_m). The mass-transfer parameter calibrated by tracer-test analysis has been reported in the literature for a number of field tracer tests; the D_m^e values calculated from the reported A values were used directly in this study. We reanalyzed those tracer tests with unavailable A values, and the resultant D_m^e values were used together with the reported D_m^e values. Based on our criteria, a number of field tracer tests and field environmental tracer observations (that provided high-quality data) were used for this investigation. Forty values of effective matrix diffusion coefficient at 15 geologic sites were obtained. To focus exclusively on the scaling effects from the fracture rock characteristics, the effective matrix-diffusion-coefficient factor (F_D), defined as the ratio of D_m^e to the lab-scale matrix diffusion coefficient, was calculated for each D_m^e value.

Survey results indicate that the effective matrix diffusion coefficients in the field are larger than the matrix-diffusion-coefficient values at the laboratory core scale, as indicated by the F_D value being generally larger than one. Furthermore, a possible trend toward systematic increase of the effective matrix diffusion coefficient with observation scale is obtained, indicating that the effective matrix diffusion coefficient, just like dispersivity and permeability [*Neuman*, 1990; *Gelhar et al*., 1992], is likely to be scale dependent. The determined F_D values range from 1 to 10,000 for scales ranging from 5 to 2,000 m. At a given scale, the F_D value varies by two orders of magnitude, reflecting the influence of differing degrees of fractured rock heterogeneity at different sites. Also, the survey results show that the field-scale longitudinal dispersivity appears to increase with observation scale, in a manner that is consistent with previous studies. These scale-dependent field-scale matrix diffusion coefficients (and dispersivities) may have significant implications for assessing long-term, large-scale radionuclide/contaminant

transport events in fractured rock sites, both for nuclear waste disposal and contaminant remediation.

Acknowledgment

We are indebted to Guoping Lu and Daniel Hawkes at Lawrence Berkeley National Laboratory for their careful review of a preliminary version of this manuscript. This work is supported by Office of Science and Technology and International, Office of Civilian Radioactive Waste Management, U.S. Department of Energy.

References

Abelin, H., L. Birgersson, J. Gidlund, I. Neretnieks, A large-scale flow and tracer experiment in granite, 1. Experimental design and flow distribution, *Water Resour. Res.,* 27(12), 3107–3117, 1991a.

Abelin, H., L. Birgersson, L. Moreno, H. Widen, T. Agren, and I. Neretnieks, A large-scale flow and tracer experiment in granite, 2. Results and interpretation, *Water Resour. Res*., 27(12), 3119–3135, 1991b.

Andersson, P., J. Byegård, E. Tullborg, T. Doe, J. Hermanson, and A. Winberg, In situ tracer tests to determine retention properties of a block scale fracture network in granitic rock at the Äspö Hard Rock Laboratory, Sweden, *J. Contam. Hydrol*., 70 (3-4), 271-297, 2004.

Altman, S. J., M. Uchida, V. C. Tidwell, C. M. Boney, and B. P. Chambers, Use of X-ray absorption imaging to examine heterogeneous diffusion in fractured crystalline rocks, *J. Contam. Hydrol*., 69, 1-26, 2004.

Bajracharya, K., and D.A. Barry (1997), Nonequilibrium solute transport parameters and their physical significance: Numerical and experimental results, J. Contam. Hydrol., 24, 185-240.

Bales, R. C., C. P. Gerba, G. H. Grondin, and S. L. Jensen, Bacteriophage transport in sandy soil and fractured tuff, *Applied and Environmental Microbiology*, 55(8), 2061–2067, 1989.

Barton, C. C., and E. Larsen, Fractal geometry of two-dimensional fracture networks at Yucca Mountain, southwestern Nevada, p. 77–84, in *Proc. Int. Symp. On Fundamentals of Rock Joints*, Bjorkliden, Sweden, 1985.

Baumle, R., Geohydraulic characterization of fractured rock flow regimes, PhD thesis, Department of Applied Geology, University of Karlsruhe, Germany, 2003.

Becker, M. W., and R. J. Charbeneau, First-passage-time transfer functions for groundwater tracer tests conducted in radially convergent flow, *J. Contam. Hydrol*., 40, 299–310, 2000.

Becker, M. W., and A. M. Shapiro, Tracer transport in fractured crystalline rock: Evidence of non-diffusive breakthrough tailing, *Water Resour. Res*., 36(7), 1677–1686, 2000.

Becker, M. W., P. W. Reimus, and P. Vilks, Transport and attenuation of carboxylate-modified-latex microspheres in fractured rock laboratory and field tracer tests, *Ground Water,* 37(3), 387–395, 1999.

Becker, M. W., and A. M. Shapiro, Interpreting tracer breakthrough tailing from different forced-gradient tracer experiment configurations in fractured bedrock, *Water Resour. Res*., 39(1), 1024, doi:10.1029/2001WR001190, 2003.

Bibby, R., Mass transport of solutes in dual-porosity media, *Water Resour. Res*., 17, 1075–81, 1981.

Birgersson, L., and I. Neretnieks, Diffusion in the matrix of granitic rock: field test in the Stripa mine, *Water Resour. Res*., 26(11), 2833–2842, 1990.

Birgersson, L., L. Moreno, I. Neretnieks, H. Widén, and T. Ågren, A tracer migration experiment in a small fracture zone in granite, *Water Resour. Res*., 29(12), 3867–3878, 1993.

Black, J. H., and K. L. Kipp, Jr., Movement of tracers through dual-porosity media—Experiments and modeling in the Cretaceous Chalk, England**,** *J. Hydrol*., 287–312, 1983.

Boving, T. B., and P. Grathwohl, Tracer diffusion coefficients in sedimentary rocks: Correlation to porosity and hydraulic conductivity, *J. Contam. Hydrol.*, 53, 85–100, 2001.

Brettmann, K. L., K. H. Jensen, and R. Jakobsen, Tracer test in fractured chalk, 2. Numerical analysis, *Nordic Hydrol*., 24, 275–296, 1993.

Brouyère, S., A. Dassargues, and V. Hallet, Migration of contaminants through the unsaturated zone overlying the Hesbaye chalky aquifer in Belgium: a field investigation, *J. Contam. Hydrol*., 72(1–4), 135–164, 2004.

Brown, S. R., and C. H. Scholz, Closure of random elastic surfaces in contact, *J. Geophys. Res*., 90, 5531–5545, 1985.

Bullivant, D. P., and M. J. O'Sullivan, Matching a field tracer test with some simple models, *Water Resour. Res*., 25, 1879–1891, 1989.

Cacas, M. C., E. Ledoux, G. de Marsily, B. Tillie, A. Barbreau, E. Durand, B. Feuga, and P. Peaudecerf, Modeling fracture flow with a stochastic discrete fracture network: Calibration and validation, 1. The flow model, *Water Resour. Res*., 26, 479–489, 1990a.

Cacas, M. C., E. Ledoux, G. de Marsily, A. Barbreau, P. Calmels, B. Gaillard, and R. Margritta, Modeling fracture flow with a stochastic discrete fracture network: Calibration and validation, 2. The transport model, *Water Resour. Res*., 26, 491–500, 1990b.

Cady, C., S. E. Silliman, and E. Shaffern, Variation in aperture estimate ratios from hydraulic and tracer tests in a single fracture, *Water Resour. Res.* 29(9), 2975–2982, 1993.

Callahan, T. J., P. W. Reimus, R. S. Bowman, and M. J. Haga, Using multiple experimental methods to determine fracture/matrix interactions and dispersion of nonreactive solutes in saturated volcanic tuff, *Water Resour. Res*., 36(12), 3547–3558, 2000.

Champ, D. R., and J. Schroeter, Bacterial transport in fractured rock—A field-scale tracer test at the Chalk River Nuclear Laboratories, *Water Sci. Technol*., 20(11/12), 81–87, 1988.

Claassen, H. C., and E. H. Cordes, Two-well recirculating tracer test in fractured carbonate rock, Nevada, *Hydrol. Sci. Bull*., 20(3), 367–382, 1975.

Cullen, J. J., K. J. Stetzenbach, and E. S. Simpson, Field studies of solute transport in fractured crystalline rocks near Oracle, Arizona, IAH Memoirs, Vol. XVII, Part 1: Hydrogeology of Rocks of Low Permeability, Tucson, AZ, 332–344, 1985.

D'Alessandro, M., F. Mousty, G. Bidoglio, J. Guimerà, I. Benet, X. Sánchez-Vila, M. G. Gutiérrez, and A. Y. de Llano, Field tracer experiment in a low permeability fractured medium: results from El Berrocal site, *J. Contam. Hydrol*., 26, 189–201, 1997.

Davison, C., P. Goblet, and I. Neretnieks, Tracer tests in fissured rock for model testing in INTRACOIN; Appendix 1, introductory description of tracer tests at Finnsjon and summary of important data, 1982.

de Hoog, F. R., J. H. Knight, and A. N. Stokes, An improved method for numerical inversion of Laplace transforms, *SIAM J. Sci. Stat. Comput*. 3(3), 357–366, 1982.

Detwiler, R. L., H. Rajaram, and R. J. Glass, Solute transport in variable–aperture fractures: An investigation of the relative importance of Taylor dispersion and macrodispersion, *Water Resour. Res*., 36(7), 1611–1625, 2000.

Finsterle, S., *ITOUGH2 user's guide*, Report LBNL-40040, UC-400, Lawrence Berkeley National Laboratory, Berkeley, CA, 1999.

Fleming, S. W., and R. Haggerty, Modeling solute diffusion in the presence of pore-scale heterogeneity: method development and an application to the Culebra dolomite Member of the Rustler Formation, New Mexico, USA, *J. Contam. Hydrol.,* 48, 253–276, 2001.

Foster, S. D., The chalk groundwater tritium anomaly—A possible explanation, *J. Hydrol.*, 25, 159–165, 1975.

Frost, L. H., N. W. Scheier, E. T. Kozak, and C. C. Davison, Solute transport properties of a major fracture zone in granite, in Hotzland, W. (eds.), Tracer Hydrology, 313–320, 1992.

Frost, L. H., N. W. Scheier, and C. C. Davison, Transport properties in highly fractured rock experiment—Phase 2 tracer tests in fracture zone 2, At. Energy of Can. Ltd., Mississauga, Ontario, 65 pp., 1995.

García Gutiérrez, M. G., J. Guimerà, A. Yllera de Llano, A. Hernàndez Benitez, J. Humm, and M. Saltink, Tracer test at El Berrocal site, *J. Contam. Hydrol.,* 26, 179–188 ,1997.

Garnier, J. M., N. Crampon, C. Préaux, G. Porel, and M. Vreulx, Traçage par 13C, 2H, I- et uranine dans la nappe de la craie sénonienne en écoulement radial convergent (Béthune, France), *J. Hydrol.,* 78, 379–392, 1985.

Gelhar, L. W., C. W. Welty, and K. R. Rehfeldt, A critical review of data on field-scale dispersion in aquifers, *Water Resour. Res.,* 28(7), 1955–1974, 1992.

Grisak, G. E., and J. F. Pickens, Solute transport through fractured media: 1. The effect of matrix diffusion, *Water Resour. Res*., 16(4), 719–730, 1980.

Grove, D. B., and W. A. Beetem, Porosity and dispersion constant calculations for a fractured carbonate aquifer using the two-well tracer method, *Water Resour. Res*., 7(1), 128–134, 1971.

Gustafsson, E., and C. E. Klockars, Studies of groundwater transport in fractured crystalline rock under controlled conditions using nonradioactive tracers, KBS 81–07, 1981.

Gustafsson E., and P. Andersson, Groundwater flow conditions in a low-angle fracture zone at Finnsjon, Sweden, *J. Hydrol.*, 126, 79–111, 1991.

Gylling, B., L. Birgersson, L. Moreno, and I. Neretnieks, Analysis of a long-term pumping and tracer test using the channel network model, *J. Contam. Hydrol*., 32, 203–222, 1998.

Hadermann, J., and W. Heer, The Grimsel (Switzerland) migration experiment: Integrating field experiments, laboratory investigations and modeling, *J. Contam. Hydrol.,* 21, 87–100, 1996.

Haggerty, R., and S. M. Gorelick, Multiple-rate mass transfer for modeling diffusion and surface reactions in media with pore-scale heterogeneity, *Water Resour. Res*., 31(10), 2383–2400, 1995.

Haggerty, R., S. W. Fleming, L. C. Meigs, and S. A. McKenna, Tracer tests in a fractured dolomite, 2. Analysis of mass transfer in single-well injection-withdrawal tests, *Water Resour. Res*., 37(5), 1113–1128, 2001.

Haggerty, R., C. F. Harvey, C. Freiherr von Schwerin, and L. C. Meigs, What controls the apparent timescale of solute mass transfer in aquifers and soils? A comparison of experimental results, *Water Resour. Res*., 40, W01510, doi:10.1029/2002WR001716, 2003.

Himmelsbach, T., H. Hotzl, P. Maloszewski, Solute transport processes in a highly permeable fault zone of Lindau fractured rock test site (Germany), *Ground Water*, 36(5), 792—799, 1998.

Hodgkinson, D. P., and D. A. Lever, Interpretation of a field experiment on the transport of sorbed and non-sorbed tracers through a fracture in crystalline rock, *Radioact. Waste Manag. Nucl. Fuel. Cycle*, 4 (2), 129–158, 1983.

Hoehn, E., J. Eikenberg, T. Fierz, W. Drost, and E. Reichlmayr, The Grimsel Migration Experiment: field injection–withdrawal experiments in fractured rock with sorbing tracers, *J. Contam. Hydrol.,* 34, 85–106, 1998.

Horne, R. N., and Rodriguez, Dispersion in tracer flow in fractured geothermal systems, *Geophys. Res. Lett*., 10(4), 289–292, 1983.

Ivanovich, M., and D. B. Smith, Determination of aquifer parameters by a two-well pulsed method using radioactive tracers, *J. Hydrol*., 36, 35–35, 1978.

Jakobsen, R., K. H. Jensen, and K. L. Brettmann, Tracer test in fractured chalk, 1. Experimental design and results, *Nordic Hydrol.*, 24, 263–274, 1993.

Jardine, P. M., W. E. Sanford, J. P. Gwo, O. C. Reedy, D. S. Hicks, J. S. Riggs, and W. B. Bailey, Quantifying diffusive mass transfer in fractured shale bedrock, *Water Resour. Res*., 35(7), 2015–2030, 1999.

Johns, R. A., and P. V. Roberts, A solute transport model for channelized flow in a fracture, *Water Resour. Res.,* 27(8), 1797–1808, 1991.

Johnson R. L., J. A. Cherry, and J. F. Pankow, Diffusive contaminant transport in natural clay: A field example and implications for clay-lined waste disposal sites, *Environmental Sciences and Technology*, 23(3), 340–349, 1989.

Jones, T. L., V. A. Kelley, J. F. Pickens, D. T. Upton, R. L. Beauheim, and P. B. Davies, Integration of interpretation results of tracer tests performed in the Culebra Dolomite at the Waste Isolation Pilot Plant, SAND92–1579, Sandia National Laboratories, Albuquerque, NM, 1992.

Karasaki, K., B. Freifeld, A. Cohen, K. Grossenbacher, P. Cook, and D. Vasco, A multidisciplinary fractured rock characterization study at Raymond field site, Raymond, CA, *J. Hydrol*., 236(1–2), 17–34, 2000.

Kreft, A., A. Lenda, B. Turek, A. Zuber, and K. Czauderna, Determination of effective porosities by the two-well pulse method, in *Isotope Techniques in Groundwater Hydrology*, Int. At. Energey, Agency (I.A.E.A.), Vienna, 295–312, 1974.

Lapcevic, P. A., K. S. Novakowski, and E. A. Sudicky, The interpretation of a tracer experiment conducted in a single fracture under conditions of natural groundwater flow, *Water Resour. Res*. 35(8), 2301–2312, 1999.

Lee, J. Y., J. W. Jim, J. Y. Cheon, M. J. Yi, and K. K. Lee, Combined performance of pumping and tracer tests: A case study, *Geosciences Journal*, 7(3), 237–241, 2003.

Lenda, A. and A. Zuber, Tracer dispersion in groundwater experiments, in *Isotope Hydrology*, Int. At. Energy Agency (I.A.E.A.), Vienna, 619–641, 1970.

Liu, H. H., C. B. Haukwa, C. F. Ahlers, G. S. Bodvarsson, A. L. Flint, and W. B. Guertal, Modeling flow and transport in unsaturated fractured rock: an evaluation of the continuum approach, *J. Contam. Hydrol*., 62–63, 173–188, 2003.

Liu, H. H., R. Salve, J. S. Wang, G. S. Bodvarsson, and D. Hudson, Field investigation into unsaturated flow and transport in a fault: model analyses, *J. Contam. Hydrol*., 74(1-4), 39–59, 2004a.

Liu, H. H., G. S. Bodvarsson, and G. Zhang, Scale dependency of the effective matrix diffusion coefficient, *Vadose Zone J*., 3, 312–315, 2004b.

Maloszewski, P., and A. Zuber, On the theory of tracer experiments in fissured rocks with a porous matrix, *J. Hydrol*., 79, 333–358, 1985.

Maloszewski, P., and A. Zuber, Mathematical modeling of tracer behavior in short-term experiments in fissured rocks, *Water Resour. Res.,* 26(7), 1517–1528, 1990.

Maloszewski, P., and A. Zuber, On the calibration and validation of mathematical models for the interpretation of tracer experiments in groundwater, *Advance in Water Resources,* 15, 47-62, 1992.

Maloszewski, P., and A. Zuber, Tracer experiments in fractured rocks: Matrix diffusion and the validity of models, *Water Resour. Res.,* 29(8), 2723–2735, 1993.

Maloszewski, P., A. Herrmann, and A. Zuber, Interpretation of tracer tests performed in a fractured rock of the Lange Bramke Basin, Germany, *Hydrogeol. J*., 7, 209–218, 1999.

McCabe, W. J., B. J. Barry, and M. R. Manning, Radioactive tracers in geothermal underground water flow studies, *Geothermics*, 12(2/3), 83–110, 1983.

McKay, L. D., R. W. Gillham, and J. A. Cherry, Field experiments in a fractured clay till, 2. Solute and colloid transport, *Water Resour. Res*., 29(12), 3879–3890, 1993a.

McKay, L. D., J. A. Cherry, R. C. Bales, M. T. Yahya, and C. P. Gerba, A field example of bacteriophage as tracers of fracture flow, *Environ. Sci. Technol.,* 27, 1075–1079, 1993b.

McKenna, S. A., L. C. Meigs, and R. Haggerty, Tracer tests in a fractured dolomite, 3. Double-porosity, multiple-rate mass transfer processes in multiwell convergent-flow tracer tests, *Water Resour. Res*., 37(5), 1143–1154, 2001.

Meigs, L. C., and R. L. Beauheim, Tracer tests in a fractured dolomite, 1. Experimental design and observed tracer recoveries, *Water Resour. Res*., 37(5), 1113–1128, 2001.

Moench, A. F., Convergent radial dispersion: A note on evaluation of the Laplace transform solution, *Water Resour. Res*., 27(12), 3261–3264, 1991.

Moench, A. F., Convergent radial dispersion in a double-porosity aquifer with fracture skin: Analytical solution and application to a field experiment in fractured chalk, *Water Resour. Res*., 31(8), 1823–1835, 1995.

Molz, F. J., and G. K. Boman, A stochastic interpolation scheme in subsurface hydrology, *Water Resour. Res*., 29, 3769–3774, 1993.

Molz, F. J., H. Rajaram, and S. Lu, Stochastic fractal-based models of heterogeneity in subsurface hydrology: Origins, applications, limitations, and future research questions, *Rev. Geophys*. 42, RG1002, doi:10.1029/2003RG000126, 2004.

Moreno, L. Y. W. Tsang, C. F. Tsang, F. V. Hale, and I. Neretnieks, Flow and tracer transport in a single fracture: A stochastic model and its relation to some field observations, *Water Resour. Res*., 24(12), 2033–2048, 1988.

National Research Council, *Rock fractures and fluid flow: Contemporary understanding and applications*, National Academy Press, Washington, DC, 1996.

Neretnieks, I., Diffusion in the rock matrix: An important factor in radionuclide retardation? *J. Geophys. Res*., 85(B8), 4379–4397, 1980.

Neretnieks, I., A stochastic multi-channel model for solute transport—analysis of tracer tests in fractured rock, *J. Contam. Hydrol*., 55, 175–211, 2002.

Neuman, S. P., Universal scaling of hydraulic conductivities and dispersivities in geologic media, *Water Resour. Res*., 26(8), 1749–1758, 1990.

Novakowski, K. S., The analysis of tracer experiments conducted in divergent radial flow fields, *Water Resour. Res*., 28(12), 3215–3225, 1992.

Novakowski, K. S., and P. A. Lapcevic, Field measurement of radial solute transport in fractured rock, *Water Resour. Res*., 30(1), 37–44, 1994.

Novakowski, K. S., G. V. Evans, D. A. Lever, and K. G. Raven, A field example of measuring hydrodynamic dispersion in a single fracture, *Water Resour. Res*., 21(8), 1165–1174, 1985.

Ohlsson, Y., and I. Neretnieks, *Literature survey of matrix diffusion theory and of experiments and data including natural analogues*, Tech. Rep. 95-12, Swed. Nucl. Fuel and Waste Manag. Co. (SKB) Stockholm, 1995.

Ohlsson, Y., M. Lofgren, and I. Neretnieks, Rock matrix diffusivity determinations by in-situ electrical conductivity measurements, *J. Contam. Hydrol*., 47, 117–125, 2001.

Ostensen, R. W., Tracer tests and contaminant transport rates in dual-porosity formations with application to the WIPP, *J. Hydrol*., 204(1–4), 197–216, 1998.

Pankow, J. F., R. L. Johnson, J. P. Hewetson, and J. A. Cherry, An evaluation of contaminant migration patterns at two waste disposal sites on fractured porous media in terms of the equivalent porous medium (EPM) model, *J. Contam. Hydrol*., 1, 65–76, 1986.

Polak, A., A. S. Grader, R. Wallach, and R. Nativ, Chemical diffusion between a fracture and the surrounding matrix: Measurement by computed tomography and modeling, *Water Resour. Res*., 39(4), 1106, doi:10.1029/2001WR000813, 2003.

Rasmuson, A., and I. Neretnieks, Radionuclide transport in fast channels in crystalline rock, *Water Resour. Res.*, 22(8), 1247–1256, 1986.

Raven, K. G., K. S. Novakowski, and P. A. Lapcevic, Interpretation of field tracer tests of a single fracture using a transient solute storage model, *Water Resour. Res*., 24(12), 2019–2032, 1988.

Reimus, P. W., and M. J. Haga, Analysis of tracer responses in the BULLION forced-gradient experiment at Pahute Mesa, Nevada, LA-13615-MS, Los Alamos Natl. Lab., Los Alamos, NM, 1999.

Reimus, P. W., M. J. Haga, A. I. Adams, T. J. Callahan, H. J. Turin, and D. A. Counce, Testing and parameterizing a conceptual solute transport model in saturated fractured tuff using sorbing and nonsorbing tracers in cross-hole tracer tests, *J. Contam. Hydrol*., 62–63, 613–636, 2003a.

Reimus, P., G. Pohll, T. Mihevc, J. Chapman, M. Haga, B. Lyles, S. Kosinski, R. Niswonger, and P. Sanders, Testing and parameterizing a conceptual model for solute transport in a fractured granite using multiple tracers in a forced-gradient test, *Water Resour. Res*., 39(12), 1356, doi:10.1029/2002WR001597, 2003b.

Robinson, B. A., and J. W. Tester, Dispersed fluid flow in fractured reservoirs: An analysis of tracer-determined residence time distributions, *J. Geophys. Res*., 89(B12), 10374–10384, 1984.

Roux, S., F. Plouraboue, and J. P. Hulin, Tracer dispersion in rough open cracks, *Transp. Porous Media*, 32, 97–116, 1998.

Rudolph, D. L., J. A. Cherry, and P. N. Farvolden, Groundwater flow and solute transport in fractured lacustrine clay near Mexico City, *Water Resour. Res*., 27(9), 2187–2201, 1991.

Salve, R., H. Liu, P. Cook, A. Czarnomski, Q. Hu, and D. Hudson, Unsaturated flow and transport through a fault embedded in fractured welded tuff, *Water Resour. Res.*, 40, W04210, doi:10.1029/2003WR002571, 2004.

Sawada, A., M. Uchida, M. Shimo, H. Yamamoto, H. Takahara, T. W., Doe, Non-sorbing tracer migration experiments in fractured rock at the Kamaishi Mine, Northeast Japan, *Engineering Geology*, 56, 75–96, 2000.

Scheier, N. W., L. H. Frost, and C. C. Davison, Groundwater tracer experiments in a major fracture zone in granite, In Bank, S., and Banks, D. (eds.), AIH Memories XXIV Congress Hydrogeology of Hard Rocks, Part 2, Oslo, Norway, 876–890, 1993.

Shapiro, A. M., Effective matrix diffusion in kilometer-scale transport in fractured crystalline rock, *Water Resour. Res*., 37(3), 507–522, 2001.

Shapiro, A. M., and J. R. Nicholas, Assessing the validity of the channel model of fracture aperture under field conditions, *Water Resour. Res*., 25(5), 817–828, 1989.

Sidle, R. C., B. Nilsson, M. Hansen, and J. Fredericia, Spatially varying hydraulic and solute transport characteristics of a fractured till determined by field tracer tests, Funen, Denmark, *Water Resour. Res*., 34(10), 2515–2527, 1998.

Skagius, K., and I. Neretnieks, Porosities and diffusivities of some nonsorbing species in crystalline rocks, *Water Resour. Res*., 22, 389–398, 1986.

Sudicky E. A., and E. O. Frind, Contaminant transport in fractured porous media: analytical solutions for a system of parallel fractures, *Water Resour. Res*., 18(7), 1634–1642, 1982.

Tang, D. H., E. O. Frind, and E. A. Sudicky, Contaminant transport in a fractured porous media: Analytical solution for a single fracture, *Water Resour. Res*., 17(3), 555–564, 1981.

Taylor, G. I., Dispersion of soluble matter in solvent flowing slowly through a tube, *Proc. R. Soc. London, Ser. A, 219*, 186–203, 1953.

Tester, J. N., R. L. Bivins, and R. M. Potter, Inter-well tracer analysis of a hydraulically fractured granite geothermal reservoir, *Soc. Pet. Eng. J*., 22, 537, 1982.

Tidwell, V. C., L. C. Meigs, T. L. Christian-Frear, and C. M. Boney, Effects of spatially heterogeneous porosity on matrix diffusion as investigated by X-ray absorption imaging, *J. Contam. Hydrol.,* 42, 285–302, 2000.

Tsang, C. F., Y. W. Tsang, and F. V. Hale, Tracer transport in fractures: Analysis of field data based on a variable-aperture channel model, *Water Resour. Res*., 27(12), 3095–3106, 1991.

Tsang Y. W., C. F. Tsang, I. Neretnieks, and L. Moreno, Flow and tracer transport in fractured media: A variable aperture channel model and its properties, *Water Resour. Res.*, 24(12), 2049–2060, 1988.

Webster, D. S., J. F. Procter, and J. W., Marine, Two-well tracer test in fractured crystalline rock, U.S. Geol. Surv. Water-Supply Paper, 1544-I, 1970.

Wheatcraft, S. W., and S. W. Tyler, An explanation of scale-dependent dispersivity in heterogeneous aquifers using concepts of fractal geometry, *Water Resour. Res*., 24, 566–578, 1988.

Widestrand, H., J. Byegård, G. Skarnemark, M. Skålberg, P. Andersson, and E. Wass, In situ migration experiments at Äspö Hard Rock Laboratory, Sweden: Results of radioactive tracer migration studies in a single fracture, *J. Radioanal. Nucl. Chem*. 250(3), 501–517, 2001.

Wu, Y. S., H. H. Liu, and G. S. Bodvarsson, A triple-continuum approach for modeling flow and transport processes in fractured rock, *J. Contam. Hydrol*. 73, 145–179, 2004.

Zhou, Q., H. H. Liu, G. S. Bodvarsson, and F. J. Molz, Evidence of multi-process matrix diffusion from a field tracer test in a single fracture, *Transport in Porous Media*, 2005.

Zhou, Q., J. Birkholzer, I. Javandel, and P. D. Jordan, Modeling three-dimensional groundwater flow and advective contaminant transport at a heterogeneous mountainous site in support of remediation, *Vadose Zone J*., 3, 884–900, 2004.

Zhou, Q., H. H. Liu, G. S. Bodvarsson, and C. Oldenburg, Flow and transport in unsaturated fractured rocks: effects of multiscale heterogeneity of hydrogeologic properties, *J. Contam. Hydrol*., 60 (1-2), 1-30, 2003.

Zuber, A., Theoretical possibilities of the two-well pulse method, *in isotope techniques in groundwater hydrology*, Int. At. Energy Agency (IAEA). Vienna, 277–294, 1974.

Table 1. Summary of characteristics of geologic site and tracer tests, calibrated transport parameters and effective matrix diffusion coefficient and observation scales for selected fractured geologic sites.

Site Name	References	Tracer Tests	Fractured Material	Fractured Zone Thickness (m)
1. Savannah River, SC	Webster et al., 1970	DRB 5–DRB 6	Crystalline	76.2
2. Poland, Poland	Lenda & Zuber, 1970 Zuber, 1974 Kreft et al., 1974	Well A–Well B (Test I-1) Well A–Well B (Test I-3) Well A–Well B (Test I-4) Well B–Well C (Test II-1)	Zn-Pb deposits Zn-Pb deposits Zn-Pb deposits Limestone	57 57 48 7
3. Chalk Aquifer, UK	Ivanovich & Smith, 1978 Maloszewski & Zuber, 1985	Borehole 5–Borehole 4	English chalk	13
4. Finnsjon, Sweden	Hodgkinson & Lever, 1983 Gustafsson & Andersson, 1991	G2-G2 KFI11-HFI01	Granite	Single fracture 1 m
5. Bethune, France	Garnier et al., 1985 Maloszewski & Zuber, 1990 Moench, 1995	Multi-tracer test	Chalk	15
6. Chalk River, Canada	Novakowski et al., 1985 Raven et al., 1988 Maloszewski & Zuber, 1993	CR 6–CR 11 Test 1 Test 2 Test 3 Test 5	Monzonitic geneiss	Single fracture 0.64 0.64 0.64 0.74
7. Red Gate Woods, IL	Shapiro & Nicholas, 1989 Maloszewski & Zuber, 1993	Test 070 (DH15-DH12)	Silurian dolomite	Single fracture
8. Fany-Augeres, France	Cacas et al., 1990a, b Maloszewski & Zuber, 1993	CH6-F3 CH7-F2	Granite	Flow paths
9. Grimsel, Switzerland	Hadermann & Heer, 1996 Hoehn et al., 1998		Granite	0.05
10. Lindau, Germany	Himmelsbach et al., 1998 Baumle, 2003	Flow 1 Flow 2 Flow 3 Monopole V Monopole I Monopole VI Dipole I Dipole VI Monopole IV Dipole III BL15-BL17	Granite in a fault zone	0.3–3
11. Lange Branks, Germany	Maloszewski et al., 1998	Test A (to HKLU) Test A (HKLU to A3) Test A (HKLU to HALB)	Fault zone of fractured sandstone	
12. Oak Ridge, TN	Jardine et al., 1999		Shale bedrock	2.0
13. Mirror Lake, NH	Becker & Shapiro, 2000, 2003 Shapiro, 2001	FSE9–FSE6 (Test C) Environ. tracer observation	Crystalline bedrock	Single fracture Fracture zone
14. Aspo, Sweden	Neretnieks, 2002 Andersson et al., 2004	STT1 C1/Path I C3/Path III	Crystalline rock	Single fracture Fracture network
15. Yucca Mountain, USA	Liu et al. [2003] Liu et al. [2004a]	Alcove 1 Alcove 8–Niche 3	Welded tuff Welded tuff	Fracture zone Fault zone

Matrix Porosity	Fracture Aperture (mm)	Conductivity (m/d) or Transmissivity	Flow Configuration	Pumping Rate (Injection Rate)	Tracer (Tracer Mass)
0.003	0.5	0.045	Pure Dipole	43,000 L/d	Tritium (297.44 Ci)
0.064	0.53 0.53 0.47 0.22	40.6 40.6 50.0 9.7	Pure Dipole	1,730 L/min 1,400 L/min 2,000 L/min 675 L/min	Tritium (23.0 mCi) Tritium (47.6 mCi) Tritium (1.44e+4 mCi) Tritium (9260.9 mCi)
0.15-0.4 (0.275)	0.11–0.19	0.70	Convergent	3,850 L/h	Tritium (20 mCi)
0.003	0.209 0.262	219.6 86.4	Convergent Natural-gradient	72 L/hr 3110L/d	Iodide Uranine (12.89g)
0.39–0.43 (0.4)	0.25	4.0-5.3	Convergent	20,800 L/h	Deuterium (260 g)
0.003	0.06 0.135 0.135 0.135 0.135		Pure Dipole Pure Dipole Pure Dipole Convergent Pure Dipole	11.84 L/h (9.67 L/h) 30 L/h 32 L/h 14 L/h 36.6 L/h	Tritium (3.53 mCi) Tritium (27 MBq) Uranine (100 mg) Tritium (27 MBq) Tritium (40 MBq)
0.02-0.18 (0.10)	2.90	0.02 m^2/s	Convergent	3.96 L/s	Sodium chloride
0.015	0.017–0.030	1.73E-3	Induced linear flow (Infiltration)		Cr-EDTA Iodine NaI
0.15	0.093	3.80	Weak dipole	8.93 L/h (0.56 L/h)	Uranine
0.041	0.434 0.444 0.576 0.110 0.237 0.256 0.107 0.117 0.237 0.268 0.206	 2.1–13 0.5–2.1 0.5–2.1 0.5–2.1 0.5–2.1 0.7–35 0.7–35	Natural-Gradient Natural-Gradient Natural-Gradient Natural-Gradient Convergent Convergent Pure Dipole Pure Dipole Convergent Pure Dipole Convergent	1.5 L/s 120 L/s 120 L/s 0.127 L/s 0.098 L/s 0.096 L/s 0.126 L/s 0.092 L/s 0.127 L/s 0.110 L/s 9.1L/s	Eosine (2.0 kg) Uranine (2 kg) Pyranine (0.5 kg) Pyranine (10 g) Pyranine (2 g) Pyranine (2 g) Eosine (2 g) Uranine (2 g) Uranine (2g) Pyranine (2 g) Bromide (388 g)
0.023	0.232	1296	Natural Gradient		Bromide (multi-tracer)
0.20	0.084	8.5	Natural Gradient		Bromide (multi-tracer)
0.017 0.015	0.40	4.8 m^2/d	Weak dipole Natural gradient	174 L/hr	Bromide (100 g) Tritium and CFC-12
0.004	1.40 2.77 15.0		Convergent Weak Dipole Convergent	24 L/h 2.0 L/min (0.045) 2.0 L/min	HTO (125 MBq) Tritium (140 MBq) HTO (240 MBq)
0.16 0.11–0.15			Infiltration in Unsaturated zone		Bromide Bromide and PFBA

Fitted T_0	Fitted P_e	Fitted A	D_m^e	D_m	Test Scale L (m)	F_D	α (m)	V (m/hr)	Test Duration (hr)
294 d	11.25	3.11e-4	2.69e-9	4.8e-12	538	560	48	0.076	17520
5.0 h	2.0	4.98e-3	4.26e-10	1.02e-10	22	4.2	11	4.4	65
3.4 h	3.07	24.0e-3	9.51e-09		22	92.8	7.2	6.47	65
5.3 h	23.5	4.37e-3	2.57e-10		21.3	2.5	0.91	4.02	40
7.8 h	40.4	6.93e-3	1.42e-10		41.5	1.4	1.03	5.32	100
1.5 h	12.5	2.1e-2	1.31e-10	1.0e-10	8	1.3	0.64	5.33	50
16.4 hr	160	3.44e-3	1.44e-8	2.67e-11	30	539	0.19	1.83	600
50 d	19.3	3.57e-4	2.43e-10	1.35e-12	440	180	22.8	0.37	2688
0.64 hr	50	40e-3	6.15e-10	1.0e-10	10.2	6.2	0.20	15.94	23
6.7 h	11.4	3.85e-3	1.48e-09	2.0e-10	10.6	7.4	0.93	1.58	30
5.6 h	4.0	1.83e-3	6.78e-09	2.0e-10	12.7	33.9	3.20	2.27	21
5.3 h	4.0	1.03e-3	2.15e-09	5.6e-11	12.7	38.4	3.20	2.40	23
34.5 h	4.3	1.0e-3	2.03e-09	2.0e-10	12.7	10.2	2.95	0.37	60
80.5 h	7.0	1.02e-3	2.11e-09	2.0e-10	29.8	10.6	4.26	0.37	160
27 min	31.3	6.5e-3	3.55e-8	1.5e-10	19.8	236.9	0.63	44.0	2.5
190 hr	12.5	1.42e-3	1.97e-11	6.75e-12	14	2.91	1.12	0.074	1800
11.2 hr	7.7	7.5e-3	5.52e-10	3.0e-11	16	18.4	2.08	1.43	720
19.6	19.6	19.6	2.5e-11	5.5e-11	4.9	0.45	0.25	0.25	1000
432 h	100	2.36e-3	1.56e-10	1.85e-11	346	8.4	3.46	0.80	6000
160.8 h	60	3.80e-3	4.23e-10	1.85e-11	235	22.9	3.92	1.46	
5.0 h	20	6.66e-3	2.19e-09	6.15e-11	49	35.6	2.45	9.80	
14.0 h	10	8.30e-3	1.24e-10	6.15e-11	21.4	2.0	2.14	1.53	
2.0 h	37	15.8e-3	2.07e-09	6.15e-11	11.2	33.7	0.30	5.60	20
2.13 h	37	12.9e-3	1.62e-09	6.15e-11	11.2	26.3	0.30	5.26	
0.7 h	67	15.5e-3	4.09e-10	1.85e-11	11.2	22.1	0.17	16.0	10
1.18 h	67	10.3e-3	2.18e-10	1.85e-11	11.2	11.8	0.17	9.49	
1.30 h	18	11.4e-3	1.08e-09	1.85e-11	16.2	58.4	0.90	12.46	
0.78 h	66	6.96e-3	5.17e-10	6.15e-11	16.2	8.4	0.25	20.77	
10 hr	7.2	6.38e-3	1.02e-09	8.53e-11	23	12.0	3.19	2.30	200
0.85 d	6.7	6.46e-3	1.06e-9	4.72e-11	11	22.5	1.64	0.54	1200
0.95 d	100	8.16e-3	1.69e-9		225	35.8	2.25	9.87	1200
0.95 d	50	1.16e-2	3.40e-9		330	72.0	6.60	14.47	7200
1.44 hr	60	0.178	1.39e-9	4.62e-10	6.0	3.0	0.1	4.17	480
27 hr	15	3.36e-3	1.62e-9	3.34e-11	36	48.5	2.4	1.33	400
23.5 y	8.0		3.20e-8	3.20e-12	2000	10000	250	0.010	
6.0 h	5.0		1.54e-09	2.0e-11	4.7	77	0.94	0.78	600
14.6 hr	8.5	1.35e-3	8.75e-11	2.5e-11	16	3.5	1.88	1.10	200
430 hr	4.1	4.2e-4	2.25e-10	2.5e-11	33	9.0	8.05	0.077	3000
					30	18.0			8160
					20	45.0		0.021	3840